Journal Name

ARTICLE TYPE

Cite this: DOI: 10.1039/xxxxxxxxxx

Exciton Formation in Monolayer Transition Metal Dichalcogenides

Frank Ceballos,[a] Qiannan Cui,[a] Matthew Z. Bellus[a], and Hui Zhao*[a]

Received Date
Accepted Date

DOI: 10.1039/xxxxxxxxxx

www.rsc.org/journalname

Two-dimensional transition metal dichalcogenides provide a unique platform to study excitons in confined structures. Recently, several important aspects of excitons in these materials have been investigated in detail. However, the formation process of excitons from free carriers has yet to be understood. Here we report time-resolved measurements on the exciton formation process in monolayer samples of MoS_2, $MoSe_2$, WS_2, and WSe_2. The free electron-hole pairs, injected by an ultrashort laser pulse, immediately induce a transient absorption signal of a probe pulse tuned to the exciton resonance. The signal quickly drops by about a factor of two within 1 ps and is followed by a slower decay process. In contrast, when excitons are resonantly injected, the fast decay component is absent. Based both on its excitation excess energy and intensity dependence, this fast decay process is attributed to the formation of excitons from the electron-hole pairs. This interpretation is also consistent with a model that shows how free electron-hole pairs can be about twice more effective than excitons in altering the exciton absorption strength. From our measurements and analysis of our results, we determined that the exciton formation times in these monolayers to be shorter than 1 ps.

Introduction

Two-dimensional transition metal dichalcogenides (TMDs), such as MoS_2 and WS_2, have drawn considerable attention since 2010. These materials are stable under ambient conditions and can be prepared by mechanically exfoliating them from their bulk crystal counterparts. Unlike graphene, it has been shown that in monolayer form TMDs are semiconductors with direct and large band gaps. In these atomically thin materials, the quantum mechanical confinement and reduced dielectric screening result in an enhanced Coulomb interaction between electrons and holes which leads to strong excitonic effects that dominate the optical response.

During the past several years, significant progress has been made in understanding several aspects of excitons in TMDs. For example, absorption, photoluminescence, and nonlinear optical studies have revealed large exciton binding energies on the order of several hundred millielectronvolts in monolayers of MoS_2 [1,2], WS_2 [2–6], $MoSe_2$ [2,7], and WSe_2 [2,8]. Large binding energies of charged excitons (trions) have also been discovered [6,9–14]. To further develop a better understanding of the energy relaxation, recombination, and real-space transport of excitons, time-resolved measurements, such as transient absorption [15–23], transient THz spectroscopy [24] and time-resolved photoluminescence [24–29] have been conducted. Strong interactions between excitons have been revealed by observations of exciton-exciton annihilation [3,19,30] and formation of biexcitons [31,32]. Furthermore, the coherent properties of excitons have also been illustrated in several measurements [13,33]. In addition, spin and valley properties of excitons have been investigated by polarization resolved spectroscopy measurements [13,17,26,34–40].

Despite of these extensive efforts, one of the key processes that determine the excitonic effect, the exciton formation, is still yet to be understood. After photoexcitation, the electron-hole pairs that carry an additional energy need to cool down in order to form excitons. This process has important implications for various optoelectronic applications such as solar cells and photodetectors.

Here we show that in monolayers of MoS_2, $MoSe_2$, WS_2, and WSe_2, the transient absorption signal decay occurs in two different temporal regions; namely, a fast decay region that lasts about one picosecond followed by a slow decay region lasting from tens to hundreds of picoseconds. We find that the formation of excitons from free electron-hole pairs explains the rapid drop of the transient absorption signal, while the slow decay component is interpreted as the exciton recombination. By fitting the fast decay region of the signal, we determine that the exciton formation times are shorter than 1 ps in all of these materials.

[a] Department of Physics and Astronomy, The University of Kansas, Lawrence, Kansas 66045, USA. Fax: 1 785 864 5262; Tel: 1 785 864 1938; E-mail: huizhao@ku.edu.

Experimental Section

TMD bulk crystals were mechanically exfoliated onto clear and flexible polydimethylsiloxane (PDMS) substrates using adhesive tape. The PDMS, placed on top of a glass slide, is then inspected with the use of an optical microscope. The monolayer flakes were first identified by optical contrast and later confirmed with photoluminescence (PL) measurements. The TMD monolayers were then manually transferred, using a micromanipulator and microscope, from the PDMS substrate onto a silicon wafer covered with 90 nm of silicon dioxide. Finally, the samples were thermally annealed at 200 °C for 2 h under a H_2/Ar (20 sccm/100 sccm) environment at a pressure of about 3 Torr.

In the transient absorption setup, a diode laser with a wavelength of 532 nm and a power of 10 W is used to pump a Ti-sapphire laser pulsing at a repetition rate of about 80 MHz. The pulses generated are centered at 770, 780, 785, or 810 nm with an average power of 2 W and have 100 fs duration. Part of this beam (a few percent) was sent into a beta barium borate (BBO) crystal to generate second harmonic or into a photonic crystal fiber for supercontinnum generation, which produces an output with a very broad spectral width. To select the desired spectral component generated from the photonic crystal fiber, bandpass filters with a bandwidth of 10 nm were utilized. The majority of the Ti-sapphire output beam was sent into an optical parametric oscillator that generates a tunable infrared output beam. Finally, a different BBO crystal was used to generate the second harmonic of the infrared beam from which we obtained either a 620 nm, 655 nm, or a 745 nm beam. Depending on the monolayer sample to be measured, different combinations of these beams were used in different configurations.

After selecting a pump-probe configuration, the pump beam intensity was modulated at about 2 KHz by a mechanical chopper. The beams were linearly polarized along perpendicular directions, combined by a beamsplitter, and focused on the sample to spot sizes of 1 - 2 μm in full width at half maximum by a microscope objective lens. The collimated reflected beams are then sent to a biased silicon photodiode connected to a lock-in amplifier that reads its output. The pump beam is prevented from reaching the detector by using a set of filters.

In all the transient absorption measurements, the sample was at room temperature. For a certain measurement, a pump pulse with a pre-selected wavelength injected free electron-hole pairs or excitons in the sample. These carriers and excitons are monitored by measuring the differential reflection of the probe pulse tuned to the peak of the A-exciton resonance of the sample. The differential reflection is defined as the pump-induced relative change of the probe reflection, $\Delta R/R_0 = (R-R_0)/R_0$, where R and R_0 are the probe reflection with and without the presence of the pump pulse, respectively. To measure the differential reflection as a function of probe delay, the pump beam path is changed by using a linear motor stage.

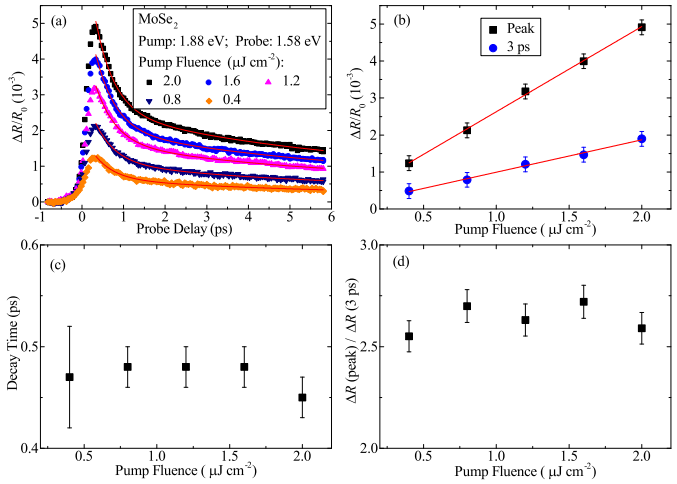

Fig. 1 (a) Differential reflection signal of monolayer $MoSe_2$ measured with pump and probe pulses of 1.88 and 1.58 eV, respectively. The pump fluences are shown in the legend. The red curves are biexponential fits. (b) The peak differential reflection (black squares) and that with a probe delay of 3 ps (blue circles) as a function of the pump fluence. The red lines are linear fits. No pump fluence dependence is observed in (c) the short time constants obtained from the biexpontential fits and (d) in the ratio between the peak differential reflection and the signal at 3 ps.

Results and Discussion

Ultrafast Transient Absorption of Monolayer $MoSe_2$

We first present results from monolayer $MoSe_2$ samples. Figure 1a shows the differential reflection signal over a short time scale with a pump pulse of 1.88 eV (660 nm) and a probe pulse of 1.58 eV (785 nm). The values of the pump energy fluence are labeled in the figure. The signal reaches a peak right after the pump excitation, limited by the instrumental response, and decays quickly for about 1 ps. This fast decay process is the main topic of this study. The black squares in Figure 1b show that the peak signal increases linearly with the pump fluence. By using an absorption coefficient[2] of 2×10^5 cm^{-1}, we estimate that the largest pump fluence used in this study, 2 μJ cm^{-2}, injects a peak areal carrier density of 10^{11} cm^{-2}. The decay of the signal after the peak is fit by a biexponential function. The deduced short and long time constants are both independent of the pump fluence in this range. Figure 1c shows the short time constants in the range of 0.45 to 0.50 ps, while the long time constants (not shown) are in the range of 5 - 6 ps. These observations show that the dynamics of the photocarriers are independent of the carrier density in such a low density regime. As a consequence, the signal at a probe delay of 3 ps (that is, after the fast-decay process) is also proportional to the pump fluence (blue cirlces in Figure 1b); therefore, the ratio between the peak signal and that at 3 ps, which we use to describe the relative strength of this fast-decay component, is independent of the pump fluence (Figure 1d). We note that the slow decay process has been generally observed in TMD monolayers, and was attributed to recombination of excitons. Since the radiative recombination of bright excitons inside the light cone can be rather fast[41,42], the relatively slow decay is

likely caused by nonradiative recombination of the whole exciton population.

To understand the origin of this fast-decay component, we measured the differential reflection signal with different pump photon energies, which define the initial states of the photocarriers. Pump photons with an energy larger than the band gap inject free electron-hole pairs, while those with an energy smaller than the band gap but larger than the exciton energy inject excitons. A few examples of the measured differential reflection signals are shown in Figure 2a. In these measurements, a portion of the 785-nm output of a Ti:sapphire laser (about 100 fs) was used as the probe, while the rest was coupled to a photonic-crystal fiber to generate coherent supercontinuum. Dielectric interference bandpass filters with a transmission bandwidth of 10 nm and various center wavelengths were used to select pump pulses with desired wavelengths. Since the supercontinuum is highly chirped, these pump pulses have slightly different pulse widths and different time delays. Dispersive elements in the pump arm also alters the pulse width and time delay differently. Typical temporal widths of the pulses obtained with this method are in the range of 300 - 400 fs; however, no efforts were made to accurately determine the temporal width and delay time of each pump pulse during the actual measurement. Consequently, the zero probe delays labeled in Figure 2a are defined somewhat arbitrarily. Previous measurements on TMD monolayers have indicated that the rising time of the transient absorption signal is typically pulse-width limited[15–23]. Hence, the rising part of the signal reflects the pulse widths of each measurement. The uncertainty on the probe delay does not impact our analysis which only involves the peak signal and the signal at 3 ps; both quantities are mostly insensitive to uncertainties in the probe delay. In these measurements, as the pump wavelength was varied, the pump fluence was adjusted so that the signal at 3 ps was maintained at the same level.

Figure 2a shows clearly that the relative strength of this fast decay component depends strongly on the pump photon energy. With low energy pump photons, this component is hardly visible while the high energy pump photons produce large magnitudes of this component. To quantitatively evaluate this effect, we compute the ratio between the peak signal and that at 3 ps, $\Delta R(\text{peak})/\Delta R(3\text{ ps})$, from these curves as well as many others that are not shown. The results are shown by the black squares in Figure 2b while the gray curve shows the photoluminescence (PL) measured from the same sample which matches the A exciton resonance (black dashed line) deduced from reflection spectroscopy[43]. The higher energy B and C exciton resonances[43] are indicated by the red and blue dashed lines, respectively.

Currently, the band gaps of TMD monolayers are still under debate. In $MoSe_2$, exciton binding energies of 0.24 and 0.55 eV has been deduced by using different techniques[2,7]. With the A-exciton resonance of 1.56 eV, these values correspond to band gaps of 1.80 and 2.11 eV and are indicated by the orange and green lines in Figure 2b, respectively. When pumping with a photon energy of 1.65 eV, pink triangles in Figure 2a, the fast component is largely absent and the signal simply decays exponentially. With an excess energy of 0.09 eV, it is safe to assume that only A-excitons are injected; hence, the decay reflects the loss of the exciton population over time. The ratio of the signals at the peak and at 3 ps is about 1.6 (Figure 2b) and agrees well with the decay time of 6 ps that further confirms the absence of the fast component. By increasing the pump photon energy, this ratio jumps to 2.2 at about 1.75 eV and slowly increases to about 2.8 as the pump photon energy is raised up to 2.5 eV.

Exciton Formation as the Origin of the Fast Decay

We argue that the data presented in Figures 1 and 2 show that the fast-decay component originates and displays the formation of excitons from the injected electron-hole pairs.

First, we can rule out the movement of photocarriers out of the probe spot as the origin of the fast decay. In order for such a process to account for the observed signal drop of about 50%, the area covered by the photocarriers needs to increase by a factor of 2 in 1 ps. According to the diffusion model, the change in the area covered by the photocarriers in a duration of Δt is $16\ln(2)D\Delta t$, where D is the diffusion coefficient[44]. Considering a laser spot of 2 μm wide, the diffusion coefficient would have to be as high as 4,000 $\text{cm}^2\,\text{s}^{-1}$, corresponding to a mobility on the order of 15,000 $\text{cm}^2\,\text{V}^{-1}\text{s}^{-1}$ for such an expansion in 1 ps. These are much higher than the known values for $MoSe_2$ monolayers[45–48]. In fact, the profile of the differential reflection signal obtained at 3 ps has a similar area of the convoluted pump and probe spots.

Generally speaking, the fast decay component may have two different types of origins. It could either be induced by the rapid loss of the photocarrier population to, for example, trap states or, without any loss of photocarrier population, by decrease of the probing efficiency due to the evolution of the photocarrier distribution.

Several pieces of evidence show that the trapping mechanism is not the origin of the observed fast component.

As shown in Figure 1d, the relative strength of this component is independent of the pump fluence. If the fast decay were induced through the trapping of photocarriers by defect states, then the existence of the signal after this fast process, which decays slowly, can only be explained if the traps are full and can no longer capture more carriers. Therefore, the signal after the fast transient (roughly measured by the signal at 3 ps) would come from the remaining photocarriers. The quantity $\Delta R(\text{peak})/\Delta R(3\text{ ps})$ would be the ratio of the initially injected density and the remaining density after the trapping process. This ratio would approach infinity if the injected density is much lower than the defect density, since no carriers are expected to survive after 3 ps. Our results show that this is clearly not the case. On the other hand, in the regime where the injected density is much higher than defect density, only a negligible fraction of the injected carriers would be trapped and the fast decay component should be nearly invisible. This also contradicts our observations. Finally, if the injected density is comparable to the defect density, one would expect a significant variation of this ratio as the injected density is changed. However, we observed no dependence in our study, with the injected photocarrier densities in the range of 10^{10} - 10^{11} cm^{-2}.

The results shown in Figure 2 provide further and even stronger

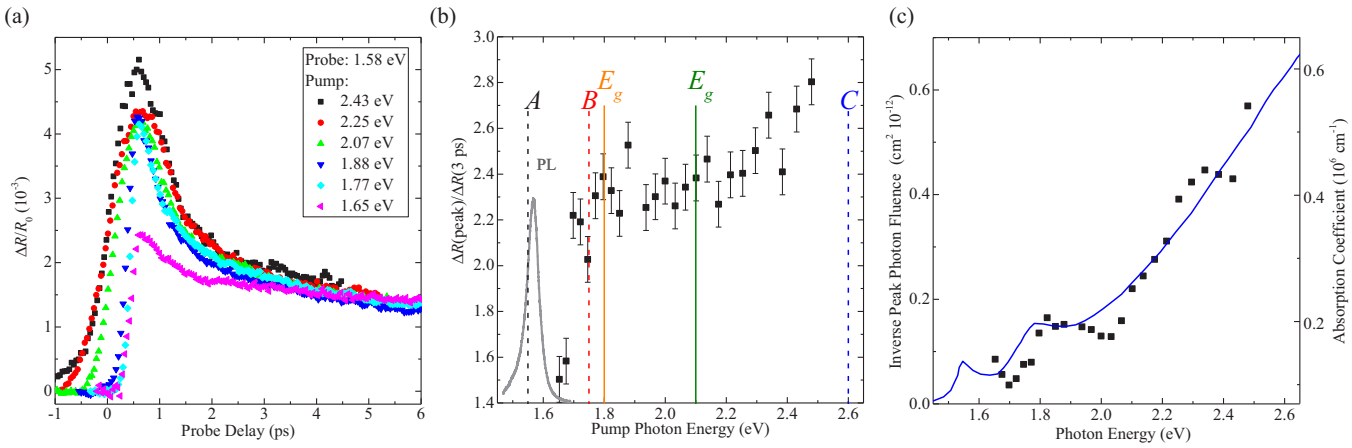

Fig. 2 (a) Differential reflection of $MoSe_2$ monolayer measured with probe and pump photon energies as labeled. A systematic variation of the short transient is seen. (b) The ratio of the peak differential reflection and that at 3 ps as a function of the pump's photon energy. The PL spectrum of the sample is shown as the gray curve. The band gaps reported are indicated by the orange[2] and green[7] solid lines. The dashed vertical lines indicate the A, B, and C exciton resonances determined by reflection spectroscopy[43]. (c) The inverse photon number fluence used in the measurement in order to maintain the differential reflection at 3 ps a constant (black squares, left axis) and the absorption coefficient of monolayer $MoSe_2$ plotted according to a previous report[2] (blue curve, right axis).

evidence to rule out the trapping process as the origin of the fast decay component. We observed a significant change of the relative strength of this fast component, from large with high pump photon energies to nearly absent when excitons are directly injected. In the measurement, we adjusted the pump fluence for each pump wavelength in order to maintain the signal at 3 ps (instead of the peak signal) to a similar level. The inverse pump fluence is plotted in Figure 2c along with the absorption coefficient of monolayer $MoSe_2$ (re-plotted from a previous report[2]). Since the product of the pump fluence and the absorption coefficient determines the injected photocarrier density, the consistency shown in Figure 2c indicates that as the pump photon energy was tuned in the measurement, the injected photocarrier density remained the same. Therefore, the signal at 3 ps, instead of the initial peak, truly reflects the injected photocarrier density. As a specific example, for the pump photon energies of 1.65 and 2.43 eV (pink triangles and black squares in Figure 2a), the pump fluence was adjusted according to the absorption coefficients at these photon energies (Figure 2c), in order for the two pulses to inject the same photocarrier density. The differential reflection signals produced at and after 3 ps are identical, but the 2.43 eV pump produces a pronounced initial peak. Hence, this initial peak is an extra feature due to the higher photon energy, instead of higher photocarrier density. As such, the initial drop of the signal is due to the loss of this extra feature, instead of a loss of photocarriers.

Without a change of the photocarrier population, the fast decay of the signal must be caused by the evolution of the injected photocarriers in energy space.

It has been well established[49] during the studies of exciton nonlinearties in quasi 2D systems, such as semiconductor quantum wells, that free electron-hole pairs can saturate the exciton oscillator strength. Since the exciton wave function is composed of free carrier states, occupation of these states alters the oscillator strength. In our measurements, pump photons with large energies inject energetic electron-hole pairs with a narrow Gaussian energy distribution. Thermalization of these carriers by intercarrier scattering rapidly converts this initial nonthermal distribution to a thermal distribution with a high temperature. In this process, carriers as a whole move from high to low energy states. Since occupying the lower energy states has a larger effect in saturating the exciton absorption, this thermalization process should induce an *increase* of the differential reflection signal. Following the thermalization process, the hot carriers relax their energy to the lattice *via* phonon scattering. Similar to thermalization, the energy relaxation process also involves the movement of carriers from high to low energy states and should be accompanied by an increase of the differential reflection signal. Hence, the thermalization and energy relaxation of carriers should have ended during the rising part of the signal and are not resolvable in our measurements. Indeed, recent measurements with higher time resolutions have revealed that these processes occur within a fraction of one picosecond after photoexcitation[50,51].

The now cooled free electron-hole pairs are expected to form excitons. During this process, the differential reflection signal could change dramatically if the free carriers and excitons are not equally efficient in saturating the exciton absorption. In particular, if the free carriers are more efficient than excitons, the signal should drop as the free carriers form excitons. Based on our observations, this appears to be the only reasonable explanation of the fast decay process. The rest of the dynamics involve excitons only, which slowly decay due to their relatively longer lifetime. Indeed, the observed step-like dependence on the pump photon energy shown in Figure 2b strongly support this assignment, since the fast decay component is largely absent when the excitons (with the same density) are directly injected. In the following paragraphs, we will show that this assignment is also quantitatively consistent with a simple and intuitive model.

Transient absorption near the exciton resonance originates

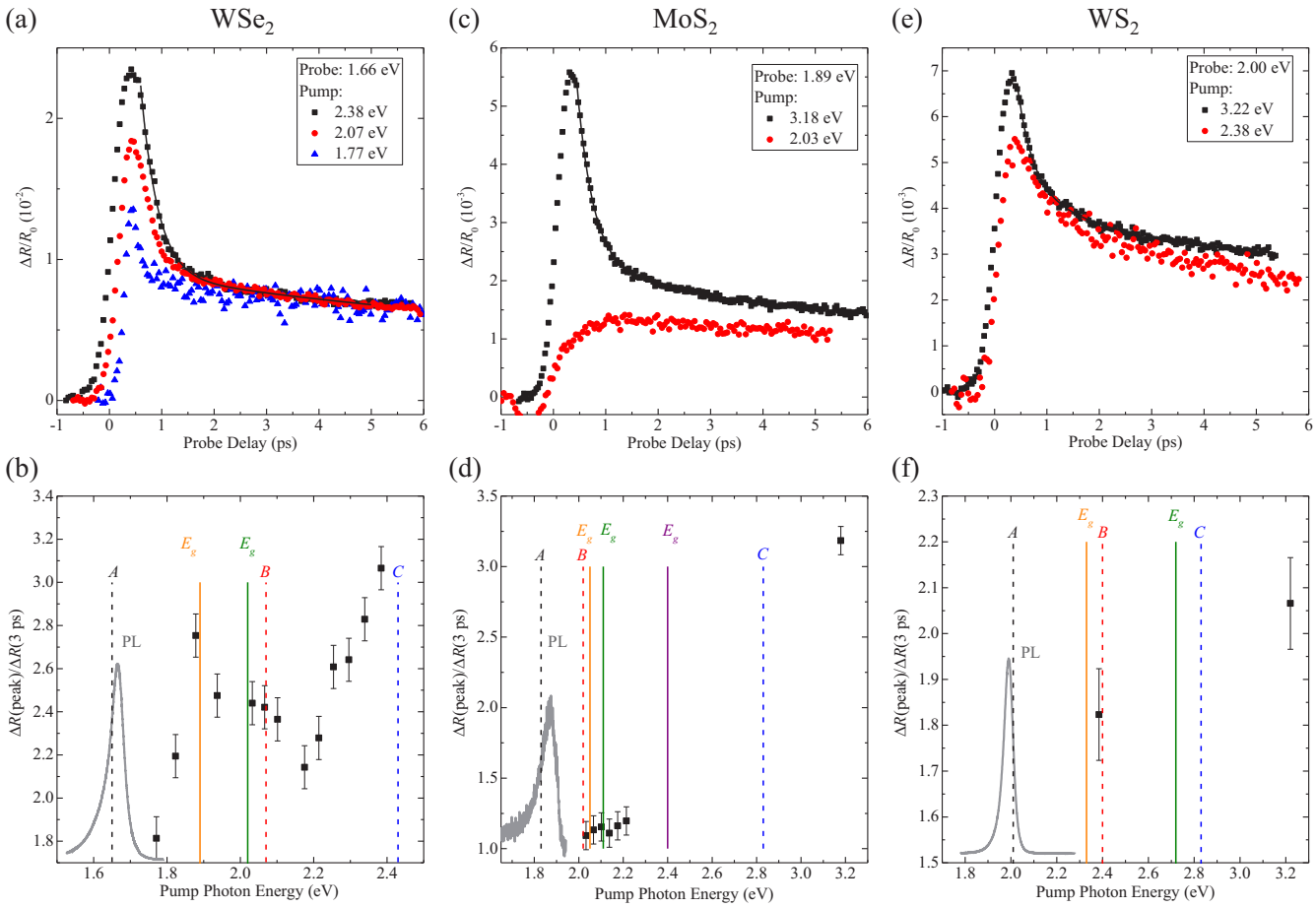

Fig. 3 (a) Differential reflection of WSe_2 monolayer measured with probe and pump photon energies as labeled. A systematic variation of the short transient is seen. (b) The ratio of the peak differential reflection and that at 3 ps as a function of the pump photon energy. The PL spectrum of the sample is shown as the gray curve. The band gaps reported are indicated as orange[2] and green[8] solid lines. (c) and (d) results of MoS_2. The band gaps are from references 1 (orange), 2 (green), and 52 (purple). (e) and (f) results of WS_2. The band gaps are from references 2,4,5 (orange) and 3,6 (green). The dashed vertical lines in (b), (d), and (f) indicate the A, B, and C exciton resonances determined by reflection spectroscopy[43].

from changes of the resonance induced by the presence of carriers or excitons. In general, these changes include saturation of the exciton oscillator strength, shift of the resonant frequency, and broadening of the linewidth. Previously, these effects in TMDs have been revealed by spectrally resolved transient absorption measurements[16,53–55]. Here, to simplify the analysis, we choose the probe photon energy to be at the peak of the absorption of the A-exciton, so that we mainly sense the saturation effect. The transient absorption, at a low carrier density, due to the saturation effect can be modeled as

$$\frac{\Delta\alpha}{\alpha_0} = \frac{\alpha(N) - \alpha_0}{\alpha_0} = -\frac{N}{N_s}, \quad (1)$$

where $\alpha(N)$ and α_0 are the absorption of the sample with the presence of photocarriers (with a density N) and without it, respectively[49]. The saturation density (N_s) describes the effectiveness of an electron-hole pair (or an exciton) on saturating the oscillator strength. We note that the linear dependence of the signal on the pump fluence, shown in Figure 1b, indicates that our experiments were performed in the regime of $N \ll N_s$.

An exciton population can reduce the oscillation strength through the phase state filling effect and the renormalization of the exciton orbital wave function, both of which originate from the exclusion principle. Based on a seminal model established by Schmitt-Rink, Chemla, and Miller[49], the inverse saturation densities, $1/N_s$, corresponding to these effects are $(32/7)\pi a_B^2$ and $(4832/1225)\pi a_B^2$, respectively, where a_B is the Bohr radius of excitons in 2D[49]. For electron-hole pairs under the condition of $k_BT \ll E_B$ where k_B, T, and E_B are Boltzmann constant, temperature, and exciton binding energy, the resulting inverse saturation densities are $8\pi a_B^2$ and $4(\pi - 2/3)\pi a_B^2$ for the phase space state filling and exchange effects, respectively[49]. In 2D TMDs, this condition is always met (at room temperature) since the exciton binding energies are on the order of several hundred millielectronvolts. By adding the two contributions, this model indicates that the inverse saturation densities of excitons and electron-hole pairs are $8.5\pi a_B^2$ and $17.9\pi a_B^2$, respectively. That is, free carriers are about twice more efficient on inducing transient absorption than excitons[49]. By noting that at 3 ps a portion of the injected photocarriers has decayed, the observed ratios of 2.2 - 2.8 are reasonably consistent with the ratio between the electron-hole pair and exciton cross sections of about two. Since the fast decay originates from exciton formation from electron-hole pairs, the decay constant of 0.47 ± 0.02 ps reflects the exciton formation rate in monolayer $MoSe_2$. Furthermore, our results appear to indicate a band gap value of about 1.80 eV, which is consistent with spectroscopic measurements[2].

We note that the model described above is based on evaluation of areas of excitons in energy space[49]. Although it is intuitive and captures the essences of excitonic nonlinearity, an accurate description of such effects requires more sophisticated models that properly include processes such as Coulomb screening and correlations beyond Hartree-Fock model[56,57]. Specifically for TMD monolayers, it was shown that Coulomb interaction and the nonparabolic bandstructure are of particular importance[58]. We hope that experimental results presented here would stimulate more sophisticated theoretical studies on this basic issue. Previous studies on conventional semiconductor structures, such as GaAs and ZnSe quantum wells, hot carriers can form excitons via optical photon emission, which is then followed by energy relaxation of hot excitons[59,60]. This process, if efficient enough in $MoSe_2$ monolayers, could contribute to the slow decay part of the signal following this initial rapid decay.

Other TMD Monolayers: WSe_2, MoS_2, and WS_2

We performed similar measurements on other TMD monolayers, including WSe_2, MoS_2, and WS_2. The results are summarized in Figure 3. As shown in Figure 3a, the relative strength of the fast component in monolayer WSe_2 also decreases significantly as the pump photon energy is decreased. The dependence of the ratio on the pump photon energy is more complicated than $MoSe_2$ and could be attributed to the different bandstructures[61]. We note that as the pump photon energy is decreases, its wavelength approaches the cutoff wavelength of the color filter that prevents the pump from reaching the detector, causing a higher level of noise. Due to the limitation of our laser system, we could only take limited data points on MoS_2, as shown in Figure 3c and d. However, it is still clearly shown that the fast component is absent with low pump photon energies. With a pump photon energy of 3.18 eV, which is safely above the band gap, the ratio is as high as 3.2. We note that a small dip was observed slightly before zero probe delay with the pump wavelength of 2.03 eV. Its origin is not understood yet; however, nonlinear interactions between the pump and the probe pulses, such as sum frequency generation and two-photon absorption, could lead to loss of probe photons and a negative differential reflection signal. Finally, we could only take two data points on WS_2, as shown as Figure 3e and f. Nevertheless, the ratio increases from 1.8 to 2.1 as the pump photon energy changed from 2.4 to 3.2 eV. From exponential fits to the fast component, as indicated by the solid black curves in Figure 3, we obtained decay time constants of 0.33 ± 0.04 ps, 0.31 ± 0.04 ps, and 0.30 ± 0.04 ps in WSe_2, MoS_2, and $MoSe_2$, respectively.

Conclusions

We observed a fast initial decay of transient absorption signal from TMD monolayers upon ultrafast interband excitation and attribute it to formation of excitons from electron-hole pairs. This conclusion is supported by the following evidence: First, this initial decay is absent when excitons are directly injected. Second, the decrease of the overall signal due to this decay, about a factor of 2, is consistent with the ratio of the cross sections of the electron-hole pairs and excitons in inducing transient absorption of the exciton resonance. Third, the relative strength of this component is independent of the injected carrier density, which rules out the defect trapping of carriers as its origin. These evidence was also observed in all the materials studied, including $MoSe_2$, MoS_2, WSe_2, and WS_2. Based on this interpretation, we are able to deduce the exciton formation time of shorter than 1 ps in these two-dimensional transition metal dichalcogenides.

Acknowledgements

This material is based upon work supported by the National Science Foundation of USA under Award Nos. DMR-1505852 and IIA-1430493.

References

1 C. Zhang, A. Johnson, C. L. Hsu, L. J. Li and C. K. Shih, *Nano Lett.*, 2014, **14**, 2443–2447.

2 H.-L. Liu, C.-C. Shen, S.-H. Su, C.-L. Hsu, M.-Y. Li and L.-J. Li, *Appl. Phys. Lett.*, 2014, **105**, 201905.

3 B. Zhu, X. Chen and X. Cui, *Sci. Rep.*, 2015, **5**, 9218.

4 H. M. Hill, A. F. Rigosi, C. Roquelet, A. Chernikov, T. C. Berkelbach, D. R. Reichman, M. S. Hybertsen, L. E. Brus and T. F. Heinz, *Nano Lett.*, 2015, **15**, 2992–2997.

5 A. Chernikov, T. C. Berkelbach, H. M. Hill, A. Rigosi, Y. L. Li, O. B. Aslan, D. R. Reichman, M. S. Hybertsen and T. F. Heinz, *Phys. Rev. Lett.*, 2014, **113**, 076802.

6 Z. Ye, T. Cao, K. O'Brien, H. Zhu, X. Yin, Y. Wang, S. G. Louie and X. Zhang, *Nature*, 2014, **513**, 214–218.

7 M. M. Ugeda, A. J. Bradley, S. F. Shi, F. H. da Jornada, Y. Zhang, D. Y. Qiu, W. Ruan, S. K. Mo, Z. Hussain, Z. X. Shen, F. Wang, S. G. Louie and M. F. Crommie, *Nat. Mater.*, 2014, **13**, 1091–1095.

8 K. He, N. Kumar, L. Zhao, Z. Wang, K. F. Mak, H. Zhao and J. Shan, *Phys. Rev. Lett.*, 2014, **113**, 026803.

9 K. F. Mak, K. He, C. Lee, G. H. Lee, J. Hone, T. F. Heinz and J. Shan, *Nat. Mater.*, 2013, **12**, 207–211.

10 J. D. Lin, C. Han, F. Wang, R. Wang, D. Xiang, S. Qin, X. A. Zhang, L. Wang, H. Zhang, A. T. Wee and W. Chen, *ACS Nano*, 2014, **8**, 5323–5329.

11 O. Lopez-Sanchez, E. A. Llado, V. Koman, A. F. I. Morral, A. Radenovic and A. Kis, *ACS Nano*, 2014, **8**, 3042–3048.

12 B. Zhu, H. Zeng, J. Dai, Z. Gong and X. Cui, *Proc. Nat. Acad. Sci. USA*, 2014, **111**, 11606–11611.

13 A. M. Jones, H. Y. Yu, N. J. Ghimire, S. F. Wu, G. Aivazian, J. S. Ross, B. Zhao, J. Q. Yan, D. G. Mandrus, D. Xiao, W. Yao and X. D. Xu, *Nat. Nanotechnol.*, 2013, **8**, 634–638.

14 Y. J. Zhang, T. Oka, R. Suzuki, J. T. Ye and Y. Iwasa, *Science*, 2014, **344**, 725–728.

15 R. Wang, B. A. Ruzicka, N. Kumar, M. Z. Bellus, H.-Y. Chiu and H. Zhao, *Phys. Rev. B*, 2012, **86**, 045406.

16 H. Shi, R. Yan, S. Bertolazzi, J. Brivio, B. Gao, A. Kis, D. Jena, H. G. Xing and L. Huang, *ACS Nano*, 2012, **7**, 1072–1080.

17 Q. Wang, S. Ge, X. Li, J. Qiu, Y. Ji, J. Feng and D. Sun, *ACS Nano*, 2013, **7**, 11087–11093.

18 H. N. Wang, C. J. Zhang and F. Rana, *Nano Lett.*, 2015, **15**, 339–345.

19 N. Kumar, Q. Cui, F. Ceballos, D. He, Y. Wang and H. Zhao, *Phys. Rev. B*, 2014, **89**, 125427.

20 J. He, D. He, Y. Wang, Q. Cui, F. Ceballos and H. Zhao, *Nanoscale*, 2015, **7**, 9526.

21 C. Mai, Y. G. Semenov, A. Barrette, Y. F. Yu, Z. H. Jin, L. Y. Cao, K. W. Kim and K. Gundogdu, *Phys. Rev. B*, 2014, **90**, 041414.

22 Q. Cui, F. Ceballos, N. Kumar and H. Zhao, *ACS Nano*, 2014, **8**, 2970–2976.

23 Q. Cui, J. He, M. Z. Bellus, M. Mirzokarimov, T. Hofmann, H.-Y. Chiu, M. Antonik, D. He, Y. Wang and H. Zhao, *Small*, 2015, **11**, 5565–5571.

24 C. J. Docherty, P. Parkinson, H. J. Joyce, M. H. Chiu, C. H. Chen, M. Y. Lee, L. J. Li, L. M. Herz and M. B. Johnston, *ACS Nano*, 2014, **8**, 11147–11153.

25 T. Korn, S. Heydrich, M. Hirmer, J. Schmutzler and C. Schueller, *Appl. Phys. Lett.*, 2011, **99**, 102109.

26 D. Lagarde, L. Bouet, X. Marie, C. R. Zhu, B. L. Liu, T. Amand, P. H. Tan and B. Urbaszek, *Phys. Rev. Lett.*, 2014, **112**, 047401.

27 G. Wang, E. Palleau, T. Amand, S. Tongay, X. Marie and B. Urbaszek, *Appl. Phys. Lett.*, 2015, **106**, 112101.

28 L. Yuan and L. B. Huang, *Nanoscale*, 2015, **7**, 7402–7408.

29 T. Yan, X. Qiao, X. Liu, P. Tan and X. Zhang, *Appl. Phys. Lett.*, 2014, **105**, 101901.

30 D. Sun, Y. Rao, G. A. Reider, G. Chen, Y. You, L. Brezin, A. R. Harutyunyan and T. F. Heinz, *Nano Lett.*, 2014, **14**, 5625–5629.

31 Y. M. You, X. X. Zhang, T. C. Berkelbach, M. S. Hybertsen, D. R. Reichman and T. F. Heinz, *Nat. Phys.*, 2015, **11**, 477–481.

32 J. Z. Shang, X. N. Shen, C. X. Cong, N. Peimyoo, B. C. Cao, M. Eginligil and T. Yu, *ACS Nano*, 2015, **9**, 647–655.

33 J. Kim, X. Hong, C. Jin, S. F. Shi, C. Y. Chang, M. H. Chiu, L. J. Li and F. Wang, *Science*, 2014, **346**, 1205–1208.

34 D. Xiao, G. B. Liu, W. Feng, X. Xu and W. Yao, *Phys. Rev. Lett.*, 2012, **108**, 196802.

35 T. Cao, G. Wang, W. P. Han, H. Q. Ye, C. R. Zhu, J. R. Shi, Q. Niu, P. H. Tan, E. Wang, B. L. Liu and J. Feng, *Nat. Commun.*, 2012, **3**, 887.

36 H. Zeng, J. Dai, W. Yao, D. Xiao and X. Cui, *Nat. Nanotechnol.*, 2012, **7**, 490–493.

37 K. F. Mak, K. He, J. Shan and T. F. Heinz, *Nat. Nanotechnol.*, 2012, **7**, 494–498.

38 S. F. Wu, C. M. Huang, G. Aivazian, J. S. Ross, D. H. Cobden and X. D. Xu, *ACS Nano*, 2013, **7**, 2768.

39 S. F. Wu, J. S. Ross, G. B. Liu, G. Aivazian, A. Jones, Z. Y. Fei, W. G. Zhu, D. Xiao, W. Yao, D. Cobden and X. D. Xu, *Nat. Phys.*, 2013, **9**, 149.

40 C. Mai, A. Barrette, Y. Yu, Y. G. Semenov, K. W. Kim, L. Cao and K. Gundogdu, *Nano Lett.*, 2013, **14**, 202–206.

41 C. Poellmann, P. Steinleitner, U. Leierseder, P. Nagler, G. Plechinger, M. Porer, R. Bratschitsch, C. Schuller, T. Korn and R. Huber, *Nat. Mater.*, 2015, **14**, 889–893.

42 C. Robert, D. Lagarde, F. Cadiz, G. Wang, B. Lassagne, T. Amand, A. Balocchi, P. Renucci, S. Tongay, B. Urbaszek and X. Marie, *ArXiv e-prints*, 2016, 1603.00277.

43 Y. Li, A. Chernikov, X. Zhang, A. Rigosi, H. M. Hill, A. M. van der Zande, D. A. Chenet, E.-M. Shih, J. Hone and T. F. Heinz, *Phys. Rev. B*, 2014, **90**, 205422.

44 L. M. Smith, D. R. Wake, J. P. Wolfe, D. Levi, M. V. Klein,

J. Klem, T. Henderson and H. Morkoç, *Phys. Rev. B*, 1988, **38**, 5788–5791.

45 N. R. Pradhan, D. Rhodes, Y. Xin, S. Memaran, L. Bhaskaran, M. Siddiq, S. Hill, M. A. P and L. Balicas, *ACS Nano*, 2014, **8**, 7923–7929.

46 J. S. Rhyee, J. Kwon, P. Dak, J. H. Kim, S. M. Kim, J. Park, Y. K. Hong, W. G. Song, I. Omkaram, M. A. Alam and S. Kim, *Adv. Mater.*, 2016, **28**, 2316–2321.

47 M. I. Utama, X. Lu, D. Zhan, S. T. Ha, Y. Yuan, Z. Shen and Q. Xiong, *Nanoscale*, 2014, **6**, 12376–12382.

48 N. Kumar, Q. Cui, F. Ceballos, D. He, Y. Wang and H. Zhao, *Nanoscale*, 2014, **6**, 4915–4919.

49 S. Schmitt-Rink, D. S. Chemla and D. A. B. Miller, *Phys. Rev. B*, 1985, **32**, 6601–6609.

50 Z. Nie, R. Long, L. Sun, C. C. Huang, J. Zhang, Q. Xiong, D. W. Hewak, Z. Shen, O. V. Prezhdo and Z. H. Loh, *ACS Nano*, 2014, **8**, 10931–10940.

51 A. G. Cabo, J. A. Miwa, S. S. Gronborg, J. M. Riley, J. C. Johannsen, C. Cacho, O. Alexander, R. T. Chapman, E. Springate, M. Grioni, J. V. Lauritsen, P. D. C. King, P. Hofmann and S. Ulstrup, *Nano Lett.*, 2015, **15**, 5883–5887.

52 A. R. Klots, A. K. Newaz, B. Wang, D. Prasai, H. Krzyzanowska, J. Lin, D. Caudel, N. J. Ghimire, J. Yan, B. L. Ivanov, K. A. Velizhanin, A. Burger, D. G. Mandrus, N. H. Tolk, S. T. Pantelides and K. I. Bolotin, *Sci. Rep.*, 2014, **4**, 6608.

53 S. Sim, J. Park, J.-G. Song, C. In, Y.-S. Lee, H. Kim and H. Choi, *Phys. Rev. B*, 2013, **88**, 075434.

54 E. J. Sie, A. J. Frenzel, Y. H. Lee, J. Kong and N. Gedik, *Phys. Rev. B*, 2015, **92**, 125417.

55 G. Moody, C. K. Dass, K. Hao, C. H. Chen, L. J. Li, A. Singh, K. Tran, G. Clark, X. D. Xu, G. Berghauser, E. Malic, A. Knorr and X. Q. Li, *Nat. Commun.*, 2015, **6**, 8315.

56 S. W. Koch, N. Peyghambarian and M. Lindberg, *J Phys. C: Solid State Phys.*, 1988, **21**, 5229–5249.

57 S. Nojima, *Phys. Rev. B*, 1995, **51**, 11124–11127.

58 A. Steinhoff, M. Rosner, F. Jahnke, T. O. Wehling and C. Gies, *Nano Lett.*, 2014, **14**, 3743–3748.

59 T. C. Damen, J. Shah, D. Y. Oberli, D. S. Chemla, J. E. Cunningham and J. M. Kuo, *Phys. Rev. B*, 1990, **42**, 7434–7438.

60 I.-K. Oh, J. Singh, A. Thilagam and A. S. Vengurlekar, *Phys. Rev. B*, 2000, **62**, 2045–2050.

61 D. Kozawa, R. Kumar, A. Carvalho, K. K. Amara, W. Zhao, S. Wang, M. Toh, R. M. Ribeiro, A. H. Castro Neto, K. Matsuda and G. Eda, *Nat. Commun.*, 2014, **5**, 4543.